Available online at www.sciencedirect.com
SCIENCE DIRECT®
Journal of Molecular Catalysis A: Chemical 216 (2004) 35–43
JOURNAL OF MOLECULAR CATALYSIS A: CHEMICAL
www.elsevier.com/locate/molcata

Characterization of Fe–TiO_2 photocatalysts synthesized by hydrothermal method and their photocatalytic reactivity for photodegradation of XRG dye diluted in water

Jiefang Zhu [a], Wei Zheng [a], Bin He [a], Jinlong Zhang [a,*], Masakazu Anpo [b]

[a] *Institute of Fine Chemicals, East China University of Science and Technology, 130 Meilong Road, Shanghai 200237, P.R. China*
[b] *Department of Applied Chemistry, Graduate School of Engineering, Osaka Prefecture University, 1-1 Gakuen-cho, Sakai, Osaka 599-8531, Japan*

Received 2 September 2003; received in revised form 31 December 2003; accepted 2 January 2004

Abstract

Iron-ion-doped anatase titanium (IV) dioxide (TiO_2) samples were prepared by hydrothermal hydrolysis and crystallization in octanol-water solution. The samples were characterized by X-ray diffraction, BET-specific surface area determination, UV-Vis diffuse reflectance spectroscopy and electron paramagnetic resonance spectroscopy. UV-Vis diffuse reflectance spectra showed a slight shift to longer wavelengths and an extension of the absorption in the visible region for almost all the ion-doped samples, compared to the non-doped sample. The photocatalytic activity of those catalysts was investigated for the liquid phase photocatatlytic degradation of active yellow XRG dye diluted in water under UV and visible light irradiation. It was found that the catalysts doped with $FeCl_3$ have better catalytic activity for photodegradation of XRG than those doped with $FeCl_2$. The amount of doped iron ion plays a significant role in affecting its photocatalytic activity and iron doped with optimum content can enhance photocatalytic activity, especially under visible light irradiation.

Keywords: Titanium dioxide; Photocatalyst; Hydrothermal method; Iron ion doping; Utilization of visible light

1. Introduction

In recent years there has been an extensive interest in the use of semiconductors as photocatalysts to initiate photocatalytic reaction at their interface [1]. As a popular catalyst, TiO_2 has been widely used because of its various merits, such as optical and electronic properties, low cost, high photocatalytic activity, chemical stability and non-toxicity [2]. However, its practical application seems limited for several reasons, among which one is the low photon utilization efficiency, another is the need to use an ultraviolet (UV) excitation source. To solve these problems, the modification of these catalysts has also been attempted by doping them with various metals such as Fe, Cr, Sn, Pt, V. The presence of foreign metal species in TiO_2 is generally detrimental for the degradation of organic species in aqueous systems, though some controversial results have been reported [3–7]. It is not easy to compare among the results reported in the literature for doped samples obtained from various preparation, because the experimental conditions and the preparation methods of the samples are usually different [8]. The photocatalytic activities of the doped TiO_2 photocatalysts substantially depend on the dopant ion nature and concentration, besides the preparation methods, the thermal and reductive treatments [9–13].

Hydrothermal method has been applied to synthesize nanosized materials already, since products prepared by this method have well crystalline phase, which benefits to thermal stability of the nanosized materials. Kominami et al. have synthesized nanosized titanium (IV) dioxide in the anatase form by hydrolysis of titanium (IV) alkoxide in the toluene with water that was dissolved from the gas phase at high temperatures (150–300 °C) [14,15]. Chen et al. also have prepared TiO_2 nanocrystalline powders by similar method [16]. However, as we know, TiO_2 doped with metal through such method has not been reported. Although some researchers have prepared TiO_2 doped with Fe ion, few of them have compared the effects of different valence Fe ions precursors on the photocatalytic activity.

* Corresponding author. Tel.: +86-2164252062; fax: +86-2164252062.
E-mail address: jlzhang@ecust.edu.cn (J. Zhang).

1381-1169/$ – see front matter © 2004 Elsevier B.V. All rights reserved.
doi:10.1016/j.molcata.2004.01.008

In this paper, the preparation of TiO_2 anatase powders doped with $FeCl_3$ or $FeCl_2$ is reported. The samples have been characterized by X-ray diffractometry (XRD), specific surface area determinations, UV-Vis diffuse reflectance spectroscopy and electron paramagnetic resonance (EPR) spectroscopy. The photodegradation of active yellow XRG (1) dye was chosen as a probe reaction to measure the photocatalytic activity of different samples.

XRG:

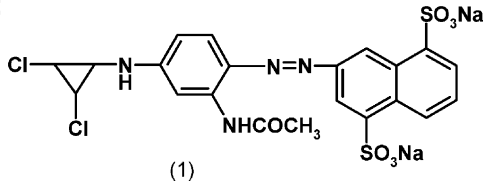

(1)

2. Experimental

2.1. Preparation of the iron-ion-doped TiO_2 photocatalysts

The iron-ion-doped TiO_2 was synthesized by the hydrothermal method. Titanium (IV) tetra-*tert*-butoxide (TTB), 4 g and the required amount of $FeCl_3$ or $FeCl_2$ were dissolved in 30 cm^3 of n-octanol in a 50 cm^3 test tube which was then set in a 160 cm^3 autoclave. An additional 30 cm^3 of deionized water was poured into the gap between the test tube and the autoclave wall. The autoclave was heated to 503 K at a rate of 2.5 K/min, and kept at 503 K for 2 h. Autogenous pressure gradually increased as the temperature was raised. After the autoclave treatment, the resulting powders were rinsed repeatedly with acetone and deionized water, until the Cl^- in the rinsing water could not be detected by 1 M $AgNO_3$ solution. The resulting powders were dried at 353 K for 8 h, and calcined at 837 K for 1 h in a box furnace under air atmosphere. In the present paper, the final samples will be denoted as $x$$FeCl_3$–$TiO_2$ or $x$$FeCl_2$–$TiO_2$, where x indicates w/w percentage of starting iron ion in theoretical product. All chemicals were of analytical grade and were used without further purification.

2.2. Characterization

XRD measurements were carried out with a Rigaku D/max 2550 VB/PC apparatus at room temperature using Cu Kα radiation and a carbon monochromator. The crystallite sizes of samples were calculated from the half-height width of different diffraction peaks of anatase using the Scherrer equation. High-purity silicon powder (99.9999%) was used as an internal standard to account for instrumental line broadening effect during crystal size estimation. Diffuse reflectance spectra (DRS) were obtained for the dry-pressed disk samples using a Scan UV-Vis-NIR spectrophotometer (Varian, Cary 500) equipped with an integrating sphere assembly, using $BaSO_4$ as reflectance sample. The spectra were recorded at room temperature in air, in the range 200–800 nm. The specific surface areas of the samples were determined through nitrogen adsorption at 77 K on the basis of BET equation (Micromeritics, ASAP2010). The X-band EPR spectra were recorded at 298 K using a Bruker ER 200D-SRC EPR spectrometer. The TiO_2 power was placed in a thin-walled quartz EPR tube to produce cylindrical samples with identical dimensions. The EPR spectrometer settings were: center field, 348.0 mT; scan range, 100.0 mT; modulation amplitude, 0.5 mT; scan time, 50 s; microwave frequency, 9.79 GHz; microwave power 6.3 mW; spectrometer gain, 1.25×10^5.

2.3. Photoactivity measurement

The photocatalytic activity of each doped TiO_2 was measured in terms of the decolorization of an active organic dye, active yellow XRG. XRG was selected because of well-defined optical absorption characteristic and good resistance to light degradation. 0.06 g of each catalyst was suspended in 60 ml of standard XRG aqueous solution (100 mg/l) using 70 ml-capacity quartz tube. The catalysts were agitated for 1 h in XRG solution in the absence of light to attain the equilibrium adsorption on the catalyst surface. UV irradiation was carried out using a 300 W high-pressure Hg lamp. The visible light (>380 nm) was achieved with a glass filter. The distance between the light and the reaction tube was 20 cm. After a given irradiation time, the samples of 3.5 ml volume were withdrawn, and the catalysts were separated from the suspensions by filtration through 0.22 μm cellulose membranes. The quantitative determination of XRG was performed by measuring its absorption at 386 nm with a UV-Vis spectrophotometer (Shimadzu UV-260). The extent of XRG photodecolorization was calculated using a calibrated relationship between the measured absorbance and its concentration. XRG can not be photodecolorized in the absence of any catalyst under the same irradiation conditions. Moreover, no further decolorization of XRG except limited absorption on the surface of the samples was observed in the dark. To determine the role of O_2 dissolved in XRG-catalysts suspensions, the photocatalytic activities of the pure TiO_2 and 0.09% $FeCl_3$–TiO_2 samples were measured in absence of O_2. In these experiments, fresh deionized distilled water was used to prepare XRG-solution, and N_2 was slowly bubbled into XRG-catalysts suspensions during dark absorption and photocatalytic reaction.

3. Results and discussion

Before our discussing the effects of doping Fe^{3+} or Fe^{2+}, the possibility of effects due to residual Cl^-, which was not washed away in the washing stage, should be considered. As we know, Cl^- has more larger ionic radius than O^{2-} (1.81 Å versus 1.40 Å), so Cl^- can not substitute O^{2-} in TiO_2 lattice. If Cl^- resided in the doped TiO_2, it must be

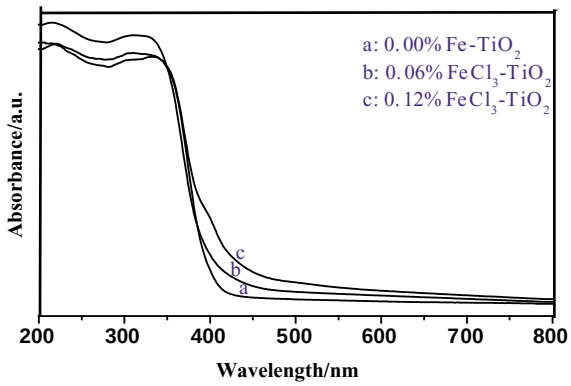

Fig. 1. UV-Vis diffuse reflectance spectra of the undoped pure TiO_2 (a), the TiO_2 doped with $FeCl_3$ with the amount of 0.06% g-Fe^{3+}/g-TiO_2 (b), and 0.12% g-Fe^{3+}/g-TiO_2 (c).

absorbed on the titania surface. Bourikas et al. investigated on a large number of different monovalent electrolytes and various ionic strength values, and concluded the interaction of the anions (including Cl^-) with the titania surface by absorption is much weaker than that of the cations [17]. Both Fe^{3+} and Fe^{2+} should have far stronger absorption on the titania surface than Cl^-, due to their higher valences. Andersson et al. used hydrochloric acid to prepare nanosize rutile TiO_2 by hydrothermal treatment of microemulsion. Although the concentration of Cl^- in that system is several hundreds higher than that in present system, and the pH value of that system is far lower than that of present system, the XPS result showed no absorbed Cl^- on the titania surface [18]. These results suggest the effects of residual Cl^- can be negligible.

UV-Vis diffuse spectra of TiO_2 doped with Fe^{3+} and Fe^{2+} are presented in Figs. 1 and 2, respectively. An abrupt increase of the absorption at shorter than 400 nm can be assigned to the intrinsic band gap absorption of pure anatase TiO_2 (~3.2 eV). It is apparent that the diffuse reflectance spectra (DRS) of all the doped TiO_2 samples have extended a red shift and increased absorbance in the visible range

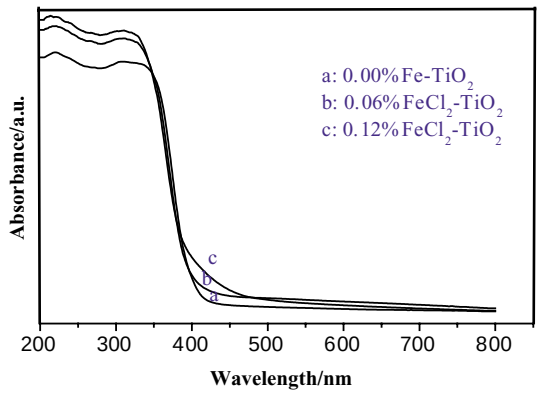

Fig. 2. UV-Vis diffuse reflectance spectra of the undoped pure TiO_2 (a), the TiO_2 doped with $FeCl_2$ with the amount of 0.06% g-Fe^{2+}/g-TiO_2 (b), and 0.12% g-Fe^{2+}/g-TiO_2 (c).

with the increasing doping content. Comparing Fig. 1 with Fig. 2, we can see samples doped with $FeCl_3$ have more remarkable absorption in visible light regions than those doped with $FeCl_2$ under the same doping content conditions. Red shift associated with the present types of dopants can be attributed to a charge transfer transition between the iron ion d electrons and the TiO_2 conduction or valence band [19]. However, it is also possible that a new absorption band in longer wavelengths region is due to the appearance of the doping ions (and/or oxide forms) as impurities, its intensity increasing with the amount of doping ions [20]. Increased light absorption in the visible region possibly leads to a better photocatalytic efficiency, especially under visible light irradiation.

Fig. 3 shows X-ray diffraction patterns for pure TiO_2 and some TiO_2 doped with iron ion. All samples exhibit only patterns assigned to the well crystalline anatase phase. Due to very low Fe content, any crystalline phase containing Fe could not be observed by XRD in Fe-doped TiO_2. For a coordination number of 6, Fe^{3+} and Ti^{4+} have similar ionic radii (0.79 Å versus 0.75 Å), so Fe^{3+} can easily substitute Ti^{4+} into TiO_2 lattice. These results support that the current doping procedure allows uniform distribution of the dopants, forming stable solid solutions within TiO_2. From the diffraction patterns it is also obvious that the materials prepared are in the form of small particles, as the peaks are broad. It can be concluded from the Scherrer equation that doping iron-ion with proper content decreases the crystal size. For example, pure TiO_2 is of the crystal size of 77.9 nm, it decreases to 11.4 nm for 0.09% $FeCl_3$–TiO_2 and 11.6 nm for 0.09% $FeCl_2$–TiO_2. These doping modifications may prevent particle agglomeration, forming well-defined nanocrystalline powders with high surface area [21]. However, a coalescence process may occur since sintering is favored by the presence of excessive dopants [22,23]. It can be seen that the crystal sizes of 0.15% $FeCl_3$–TiO_2 and 0.15% $FeCl_2$–TiO_2 are larger than those of 0.09% $FeCl_3$–TiO_2 and 0.09% $FeCl_2$–TiO_2, respectively. These observations are consistent with the values of surface area.

The specific surface areas of all samples are shown in Table 1. Reduction in particle size, which was caused by doping iron-ion within suitable concentration range led to larger surface area. The 0.09% $FeCl_3$–TiO_2 and 0.09% $FeCl_2$–TiO_2 have high specific surface areas of 101.4 and 90.5 m^2/g, respectively. Higher specific surface area may be of benefit to their high photocatalytic activity, due to enhanced adsorption of irradiation photons and dye molecules. However, undoped TiO_2 and highly-doped TiO_2 have very low-specific surface areas.

Fig. 4 shows the EPR spectra of some samples recorded at 298 K. EPR is a highly sensitive spectroscopic technique for examining paramagnetic species (levels of Fe <0.01% are detectable) and can give valuable information about the lattice site in which a paramagnetic dopant ion is located. Transition-metal ions are generally paramagnetic due to their partially filled d orbits. At room temperature, Fe^{3+} can eas-

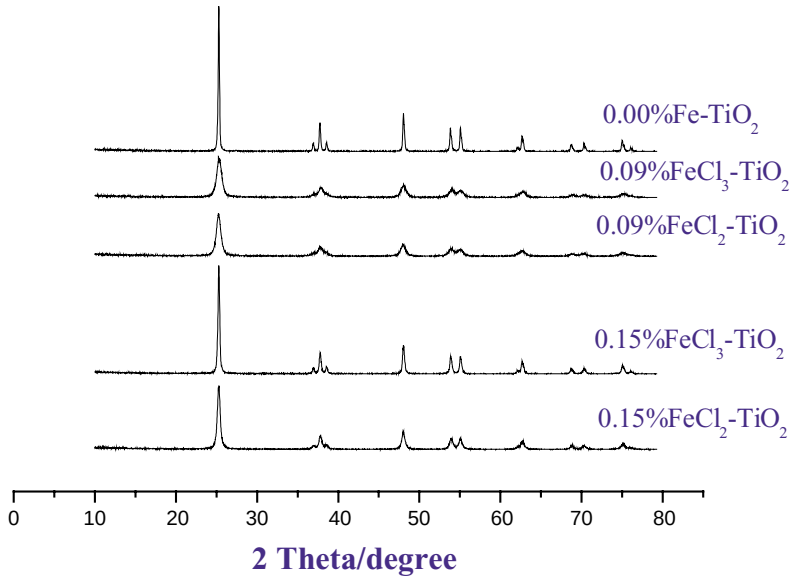

Fig. 3. X-ray diffraction patterns of the undoped pure TiO_2 and iron-ion-doped TiO_2.

Table 1
Particle characteristics and photoactivities of the undoped and doped TiO_2

Sample	Crystal phase	Crystallite size (nm)	Surface area (m^2/g)	UV-decolorized XRG(%)[a]	Vis-decolorized XRG(%)[b]
Undoped	Anatase	77.9	29.0	56.75	18.38
0.03% $FeCl_2$–TiO_2	Anatase	73.5	35.6	14.37	2.27
0.03% $FeCl_3$–TiO_2	Anatase	77.9	31.5	20.61	6.95
0.06% $FeCl_2$–TiO_2	Anatase	46.4	46.7	3.74	5.61
0.06% $FeCl_3$–TiO_2	Anatase	43.2	54.2	16.31	6.02
0.09% $FeCl_2$–TiO_2	Anatase	11.6	90.5	60.16	25.80
0.09% $FeCl_3$–TiO_2	Anatase	11.4	101.4	70.19	41.18
0.12% $FeCl_2$–TiO_2	Anatase	36.2	26.3	3.56	6.02
0.12% $FeCl_3$–TiO_2	Anatase	59.4	16.1	4.22	7.35
0.15% $FeCl_2$–TiO_2	Anatase	17.6	55.5	16.49	7.62
0.15% $FeCl_3$–TiO_2	Anatase	32.2	20.6	20.45	8.29

[a] After photodecolorization for 1 h, exclusive of equilibrium adsorption.
[b] After photodecolorization for 7 h, exclusive of equilibrium adsorption.

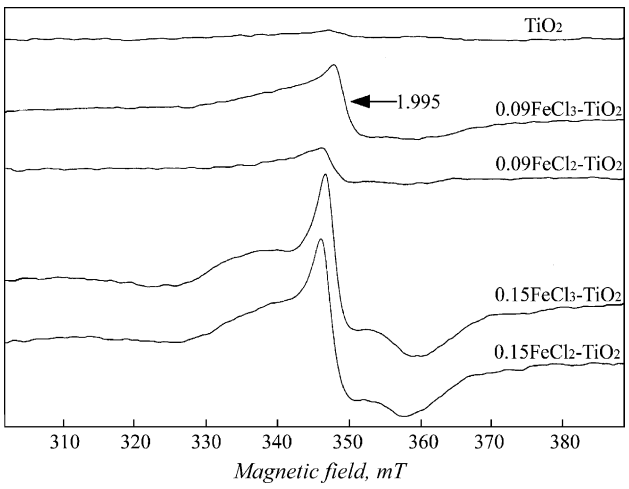

Fig. 4. EPR spectra of some samples measured at room temperature.

ily give the EPR signals, while Fe^{2+} can not, due to its very short relaxation time. From Fig. 4, we can see that all the doped samples (prepared from both $FeCl_3$ and $FeCl_2$) have the signal of $g = 1.995$, assigned to Fe^{3+}, its intensity increasing with doping content. It is significant to note that in 0.09% $FeCl_2$–TiO_2 the signal intensity is weaker than that in 0.09% $FeCl_3$–TiO_2. It can be presumed that in $FeCl_2$–TiO_2 most of Fe^{2+}, especially on and near the surface of microcrystal, were oxided to Fe^{3+} during calcinations under air atmosphere, meanwhile the rest of Fe^{2+} remained in the bulk of microcrystal. Compared to those of 0.09% Fe–TiO_2, the spectral lines of 0.15% Fe–TiO_2 look more complex. The multicomponent EPR spectra of Fe^{3+} in 0.15% Fe–TiO_2 mean that besides the same site corresponding to the signal of $g = 1.995$, in 0.15% Fe–TiO_2 there are other sites where excessive Fe^{3+} locate, which may be unfavorable to good photocatalytic activity. Investigations on the detailed microenvironment of doped iron are now in progress.

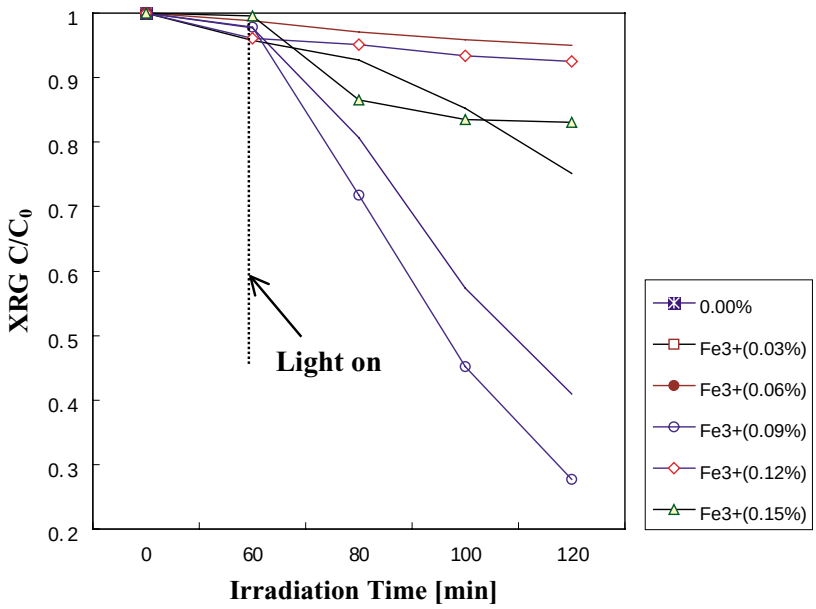

Fig. 5. Photodecolorization of XRG over $FeCl_3$–TiO_2 as a function of UV light irradiation time.

The photocatalytic decolorization of XRG was investigated by determining the remaining concentration of XRG at various time intervals. In Figs. 5–8, after the dark adsorption for first one hour was achieved, the photocatalytic decolorization of XRG was carried out. Figs. 5–8 show that the photocatalytic decolorization of XRG approximately follows zero order kinetics under both UV and visible irradiation. It is obvious that only 0.09% $FeCl_3$–TiO_2 and 0.09% $FeCl_2$–TiO_2 are more photoactive than undoped TiO_2, and 0.09% $FeCl_3$–TiO_2 has the best photocatalytic activity. It is worth noting that the amount of doped iron is very important to photoactivity, that is to say, high or low level doping decreases the photocatalytic activity markedly as shown in Figs. 9 and 10. The correlation between photocatalytic activity and dopant concentration is well consistent with the effect of dopant concentration on the specific surface areas and crystal sizes of samples, as shown in Table 1. It is believed that 0.09% $FeCl_3$–TiO_2 and 0.09% $FeCl_2$–TiO_2 should have excellent photoactivity due to high specific surface areas and small crystal sizes.

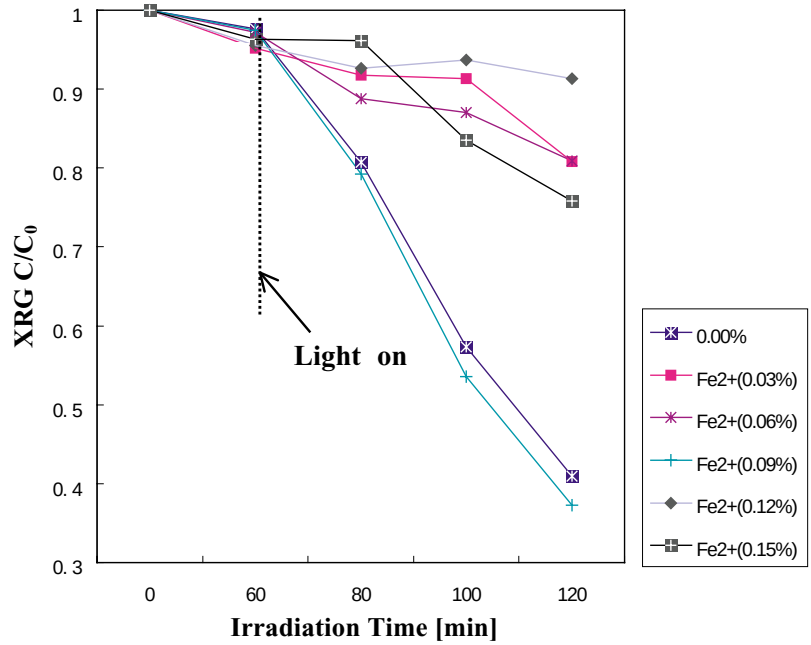

Fig. 6. Photodecolorization of XRG over $FeCl_2$–TiO_2 as a function of UV light irradiation time.

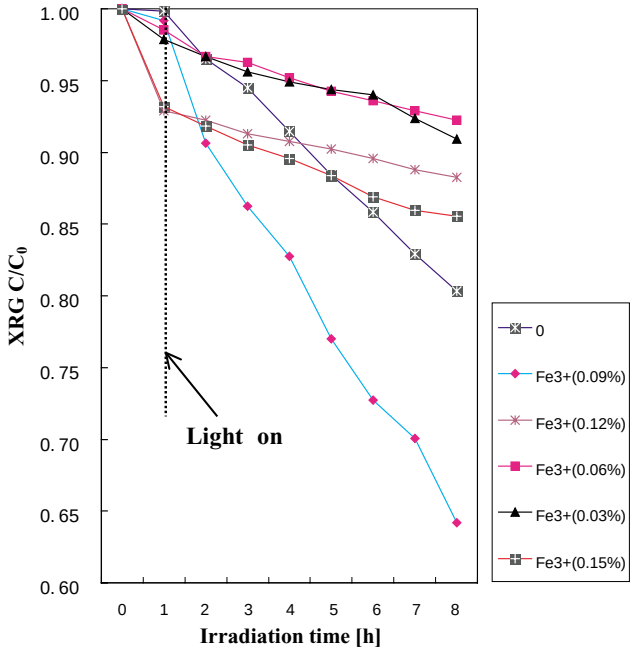

Fig. 7. Photodecolorization of XRG over $FeCl_3$–TiO_2 as a function of visible light irradiation time.

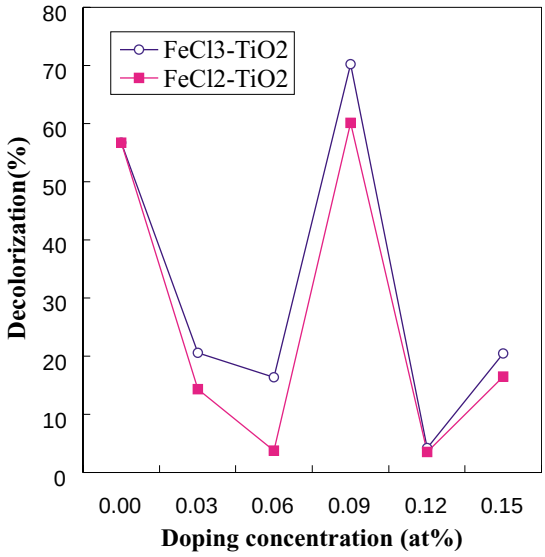

Fig. 9. Photodecolorizated amounts of XRG by the Fe-doped TiO_2 as a function of doping concentration. UV irradiation time was 60min, exclusive of equilibrium adsorption.

The photocatalytic decolorization of XRG by TiO_2 and 0.09% $FeCl_3$–TiO_2 was also investigated in absence of O_2. Under UV irradiation, the final decolorization decreases to 49.04% for pure TiO_2 and to 60.18% for 0.09% $FeCl_3$–TiO_2. The similar loss of about 14% in photocatalytic decolorization may be due to lack of O_2^- formed by absorbed O_2 reacting with photogenerated electrons (e^-) or trapped electrons. However, in this condition photogenerated holes (h^+) and $OH^\bullet$, which is formed by h^+ reacting with OH^-, should be the major active species for the reaction. Under visible light irradiation, the final decolorization decreases to 16.07% for pure TiO_2 and to 30.19% for 0.09% $FeCl_3$–TiO_2. The loss of 27% in photocatalytic decolorization by 0.09% $FeCl_3$–TiO_2 indicates that O_2^- play a more important role under visible light irradiation than that under UV irradiation. In contrast to the loss in photocatalytic decolorization by pure TiO_2, it

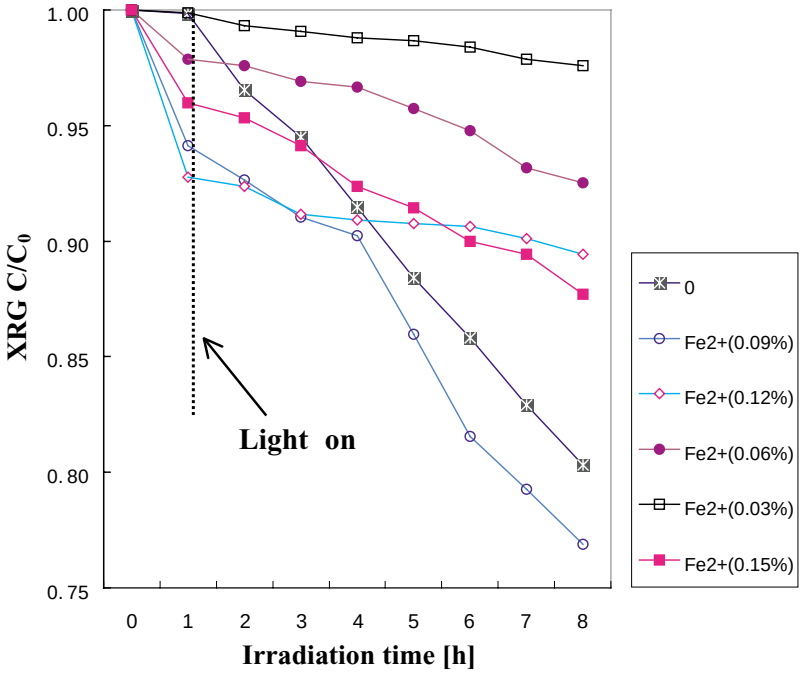

Fig. 8. Photodecolorization of XRG over $FeCl_2$–TiO_2 as a function of visible light irradiation time.

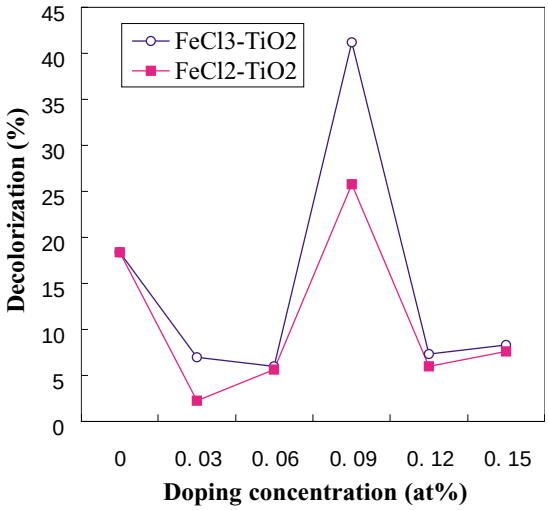

Fig. 10. Photodecolorizated amounts of XRG by the Fe-doped TiO_2 as a function of doping concentration. Visible light irradiation time was 7 h, exclusive of equilibrium adsorption.

can be concluded that iron species benefit to the formation of O_2^- under visible light irradiation. It can be proposed that in most case h^+ and $OH^\bullet$ should be the main active species, but for iron-doped samples O_2^- might act as the assistant active species effectively under visible light irradiation.

The beneficial effect of Fe^{3+} may be explained by considering the formation of Fe^{2+} species by means of a transfer of photogenerated electrons from TiO_2 to Fe^{3+} (Eq. (1)). According to the crystal field theory, Fe^{2+} is relatively unstable due to the loss of d^5 (half-filled high spin) electronic configuration, and tends to return to Fe^{3+} (d^5). Subsequently Fe^{2+} could be oxided to Fe^{3+} by transferring electrons to absorbed O_2 on the surface of TiO_2 (Eq. (2)). The Fe^{2+}/Fe^{3+} energy level lies close to Ti^{3+}/Ti^{4+} level. As a consequence of this proximity, the trapped electron in Fe^{2+} can also be easily transferred to a neighboring surface Ti^{4+} (Eq. (3)), which then leads to interfacial electron transfer. That is to say, Fe^{3+} can be an effective electron trap in anatase. Meanwhile, Fe^{3+} can also serve as hole trap (Eq. (4)), due to the energy level for Fe^{3+}/Fe^{4+} above the valence band edge (E_{vb}) of anatase TiO_2. The trapped hole embodied in Fe^{4+} has longer lifetime because of the immobilized electron in Fe^{2+} [24]. Therefore, Fe^{3+} can act as both hole and electron traps, according to the following reactions:

$$Fe^{3+} + e^- \rightarrow Fe^{2+} \quad (1)$$

$$Fe^{2+} + O_{2(ads)} \rightarrow Fe^{3+} + O_2^- \quad (2)$$

$$Fe^{2+} + Ti^{4+} \rightarrow Fe^{3+} + Ti^{3+} \quad (3)$$

$$Fe^{3+} + h_{vb}^+ \rightarrow Fe^{4+} \quad (4)$$

This hypothesis can interpret the observed higher photoactivity in $FeCl_3$–TiO_2. In $FeCl_2$–TiO_2, there might be some residual Fe^{2+} in the bulk of the samples, though during the calcinations process most of Fe^{2+} were oxided to Fe^{3+}. Compared to Fe^{3+}, Fe^{2+} can only serve as hole trap (Eq. (5)). Photoexcited electron in the presence of Fe^{2+}, which cannot trap an electron, easily recombines with a trapped hole (Eq. (6)):

$$Fe^{2+} + h_{vb}^+ \rightarrow Fe^{3+} \quad (5)$$

$$Fe^{3+} + e^- \rightarrow Fe^{2+} \quad (6)$$

Dopants should act as both electron traps and hole traps to be photoactive. Trapping either an electron or a hole alone is ineffective, because the trapped and immobilized charge specie quickly recombines with its mobile counterpart [24]. That is why doping Fe^{3+} causes better effect than doping Fe^{2+} with the same doping level.

It cannot be excluded that Fe^{3+} or Fe^{2+} in the TiO_2 lattice could also act as recombination centers for the electron–hole pair, according to the following reactions:

$$Fe^{3+} + e^- \rightarrow Fe^{2+} \quad (7)$$

$$Fe^{2+} + h_{vb}^+ \rightarrow Fe^{3+} \quad (8)$$

$$Fe^{3+} + h_{vb}^+ \rightarrow Fe^{4+} \quad (9)$$

$$Fe^{4+} + e^- \rightarrow Fe^{3+} \quad (10)$$

These reactions are in competition with the redox processes that can occur at the solid–liquid interface.

In Figs. 9 and 10, it is interesting to find that except at intermediate level (0.09%), the presence of iron species, even for low levels of doping, retards reaction. However, we can also see that the particle sizes of samples for low levels of doping are much larger than those of 0.09% $FeCl_3$–TiO_2 and 0.09% $FeCl_2$–TiO_2. It could be suggested that the optimal Fe^{3+} or Fe^{2+} dopant concentration should be strongly dependent on the particle size of the TiO_2 catalyst, and concretely speaking it should decrease with increasing TiO_2 particle size. When particle size becomes larger, the average path length of a charge carrier to the surface is longer. If the dopant concentration does not change, the possibility that a charge carrier meets a dopant increases, and so does the chance of multiple trappings. If a charge carrier is trapped more than once on its way to the surface, its apparent mobility may become extremely low and it will likely recombine with its mobile counterpart generated by subsequent photons before it can reach the surface. To reduce the possibility of multiple trappings, the dopant concentration should be decreased with increasing particle size. Zhang et al. found that the optimal Fe^{3+} concentration decreased from 0.2 at.% for the 6 nm TiO_2 to 0.05 at.% for the 11 nm sample prepared by the same wet-chemical process. They also proposed that the high photoreactivity of Degussa P25 (30 nm in its primary particle size) should be partly due to its minor Fe^{3+} impurity concentration of 0.012 at.% [24]. Choi et al. found the optimal Fe^{3+} concentration is 0.5 at.% for TiO_2 with a particle size of 2–4 nm under photocatalytic condition similar to Zhang et al.'s [25]. Our experimental results also support

this argument. In present work, although the particle sizes of TiO_2 is reduced by doping iron-ion within suitable concentration range, the particle sizes of samples are still larger than 40 nm for low levels of doping (<0.09%). Therefore, the optimal Fe^{3+} concentration for these samples is expected to be far lower than 0.01 at.%. In 0.03% $FeCl_3$–TiO_2, 0.03% $FeCl_2$–TiO_2, 0.06% $FeCl_3$–TiO_2 and 0.06% $FeCl_2$–TiO_2, the amount of dopant is relatively excessive. In these samples, Fe^{3+} or Fe^{2+} dopant hinders photongenerated electrons (e^-) and holes (h^+) migrating to the surface, and serves as recombination centers. This result may be used to explain some of the controversial results reported in previous investigations on Fe^{3+} doping, in which the detrimental effects observed might be due to the relatively high Fe^{3+} doping levels applied to the large TiO_2 particles [26,27].

Different preparation methods may result in different defect structures and surface morphologies, affecting the photocatalytic activity. The hydrothermal synthesis should become a good doping method, because dopant ions precursor distributes uniformly in reaction system during the whole hydrothermal process. The relative efficiency of a metal ion dopant depends on whether it serves as a mediator of interfacial charge transfer or as a recombination center, which is related to the preparation method, the dopant concentration, the energy level of the dopant within the TiO_2 lattice, its d electronic configuration, the distribution of the dopant within the particles [25]. It seems that Fe dopant acts as charge traps retarding electron–hole recombination and enhancing interfacial charge transfer to degrade the XRG dye adsorbed on the surface of the particles within the suitable concentration range of dopant. When the dopant concentration is too high, the recombination rate will increase because the distance between trapping sites in a particle decreases. In addition, by EPR analysis there may be some undesirable microenvironments of doped iron in excessively doped samples. It is believed that the crystal sizes and the specific surface areas of the catalysts, which were modified by doping iron ion, must play a significant role in determining the photocatalytic decolorization of XRG. These two modifications of the photocatalysts may partly explain the photocatalytic results in the present study.

From Table 1 and Figs. 9 and 10, we found that 0.09% $FeCl_3$–TiO_2 and 0.09% $FeCl_2$–TiO_2 are more photoactive than undoped sample, especially under visible light irradiation. This phenomenon indicates doping Fe ion by this method can effectively utilize visible light or solar energy. UV-Vis diffuse reflectance spectra (Figs. 1 and 2) of Fe–TiO_2 exhibiting a red shift from undoped TiO_2 perhaps provide the information on the sensitization mechanism of the iron ion doped TiO_2 photocatalysts. Anpo and co-workers have reported that in the metal ion-implanted TiO_2 the overlap of the conduction band due to Ti (d) of TiO_2 and the metal (d) orbital of the implanted metal ions could decrease the band gap of TiO_2 to enable to adsorb the visible light [28]. Visible absorption in these Fe–TiO_2 photocatalysts is possibly indicative of the excitation of a 3d electron from a Fe^{3+} center into the TiO_2 conduction band, since the energy level for Fe^{3+}/Fe^{4+} lies above the valence band edge (E_{vb}) of TiO_2. It can be believed that the visible-light-excited electron enables photocatalytic decolorization of XRG to occur at the surface of the Fe–TiO_2, as it can react with absorbed O_2 to form O_2^-, which can initiate a variety of photooxidation reactions.

4. Conclusions

It has been concluded that TiO_2 moderately doped with iron ion by hydrothermal method exhibited higher photocatalytic reactivity than undoped TiO_2 for the liquid phase photocatalytic decolorization of active yellow XRG diluted in water. The 0.09% $FeCl_3$–TiO_2 and 0.09% $FeCl_2$–TiO_2 have high specific surface areas and small crystal sizes, which are of benefit to efficient photocatalytic reactions. Fe acting as both hole and electron traps can enhance photocatalytic activity of TiO_2. The UV-Vis diffuse reflectance spectra of all the doped TiO_2 samples showed a slight red shift in the band gap transition. It is suggested that under visible light irradiation photoexcited iron centers donate electrons to TiO_2 conduction band, which allows the photocatalytic degradation of XRG. Anyway, the hydrothermal method can be applied to dope TiO_2 with metal ion deep and uniformly, which may effectively enhance photoactivity of TiO_2 and utilize the visible light.

Acknowledgements

This work has been supported by the National Nature Science Foundation of China (No. 2007306); Foundation of Ministry of Education of China (No. 01078); Shanghai Nanotechnology Promotion Center (No. 0123nm023); Commission of Education of Shanghai.

References

[1] M.R. Hoffmann, S.T. Martin, W. Choi, D.W. Bahnemann, Chem. Rev. 95 (1995) 69.
[2] A. Fujishima, T.N. Rao, D.A. Truk, J. Photochem. Photobiol. C: Photochem. Rev. 1 (2000) 1.
[3] A. Di Paola, G. Marcì, L. Palmisano, M. Schiavello, K. Uosaki, S. Ikeda, B. Ohtani, J. Phys. Chem. B 106 (2002) 637.
[4] D. Dvoranová, V. Brezová, M. Mazúr, M.A. Malati, Appl. Cat. B: Environ. 37 (2002) 91.
[5] J. Araña, O.G. Díaz, M.M. Saracho, J.M.D. Rodríguez, J.A.H. Melián, J.P. Peña, Appl. Cat. B: Environ. 36 (2002) 113.
[6] S. Klosek, D. Raftery, J. Phys. Chem. B 105 (2001) 2815.
[7] M. Takeuchi, H. Yamashita, M. Matsuoka, M. Anpo, T. Hirao, N. Itoh, N. Iwamoto, Cat. Lett. 67 (2000) 135.
[8] L. Palmisano, A. Sclafani, in: M. Schiavello (Ed.), Heterogeneous Photocatalysis, vol. 3, John Wiley & Sons, Chichester, 1997, p. 109 (Chapter 4).
[9] V. Brezová, A. Blaková, L. Karpinský, J. Groková, B. Havlínová, V. Jorík, M. Ceppan, J. Photochem. Photobiol. A: Chem. 109 (1997) 177.

[10] H. Tahiri, Y.A. Ichou, J.M. Herrmann, J. Photochem. Photobiol. A: Chem. 114 (1998) 219.
[11] A. Blaková, I. Csölleová, V. Brezová, J. Photochem. Photobiol. A: Chem. 113 (1998) 251.
[12] M.I. Litter, Appl. Catal. B: Environ. 23 (1999) 89.
[13] K. Wilke, H.D. Breuer, J. Photochem. Photobiol. A: Chem. 121 (1999) 49.
[14] H. Kominami, J. Kato, Y. Takada, Y. Doushi, B. Ohtani, S. Nishimoto, M. Inoue, T. Inui, Y. Kera, Cat. Lett. 46 (1997) 235.
[15] H. Kominami, S. Murakami, Y. Kera, B. Ohtani, Cat. Lett. 56 (1998) 125.
[16] Q.W. Chen, Y.T. Qian, Z.Y. Chen, G.E. Zhou, Y.H. Zhang, Mater. Lett. 22 (1,2) (1995) 77.
[17] K. Bourikas, T. Hiemstra, W.H. Van Riemsdijk, Langmuir 17 (2001) 749.
[18] M. Andersson, L. Österlund, S. Ljungström, A. Palmqvist, J. Phys. Chem. B 106 (2002) 10674.
[19] E. Borgarello, J. Kiwi, E. Pelizzetti, M. Visca, M. Grätzel, J. Am. Chem. Soc. 103 (1981) 6324.
[20] M. Anpo, Y. Ichihashi, M. Takeuchi, H. Yamashita, Res. Chem. Intermed. 24 (1998) 143.
[21] J. Moon, H. Takagi, Y. Fujishiro, M. Awano, J. Mater. Sci. 36 (2001) 949.
[22] G. Marcì, L. Palmisano, A. Sclafani, A.M. Venezia, R. Campostrini, G. Carturan, C. Martin, V. Rives, G. Solana, J. Chem. Soc. Faraday Trans. 92 (1996) 819.
[23] J.A. Navío, G. Colón, M.I. Bitter, G.N. Bianco, J. Mol. Cat. A: Chem. 106 (1996) 267.
[24] Z. Zhang, C. Wang, R. Zakaria, J.Y. Ying, J. Phys. Chem. B 102 (1998) 10871.
[25] W. Choi, A. Termin, M.R. Hoffmann, J. Phys. Chem. 98 (1994) 13669.
[26] L. Palmisano, V. Augugliaro, A. Sclafani, M. Schiavello, J. Phys. Chem. 92 (1998) 6710.
[27] L. Palmisano, M. Schiavello, A. Sclafani, C. Martin, I. Martin, V. Rives, Cat. Lett. 24 (1994) 303.
[28] H. Yamashita, M. Harada, J. Misaka, M. Takeuchi, K. Ikeue, M. Anpo, J. Photochem. Photobiol. A: Chem. 148 (2002) 257.